AIMS Mathematics, 8(7): 16864–16886.
DOI: 10.3934/math.2023862
Received: 17 February 2023
Revised: 23 April 2023
Accepted: 24 April 2023
Published: 15 May 2023

http://www.aimspress.com/journal/Math

Research article

The improved giant magnetostrictive actuator oscillations via positive position feedback damper

Hany Bauomy[1,2,*], A. T. EL-Sayed[3], A. M. Salem[3] and F. T. El-Bahrawy[3]

[1] Department of Mathematics, College of Arts and Science in Wadi Addawasir, Prince Sattam Bin Abdulaziz University, P.O. Box 54, Wadi Addawasir 11991, Saudi Arabia
[2] Department of Mathematics, Faculty of Science, Zagazig University, Zagazig 44519, Egypt
[3] Department of Basic Science, Modern Academy for Engineering and Technology, El-Hadaba ElWosta, Elmokattam 11439, Egypt

* **Correspondence:** Email: hany_samih@yahoo.com.

Abstract: This article contemplates the demeanor of the giant magnetostrictive actuator (GMA) when a positive position feedback (PPF) damper is used to enable tight control over its vibration. The methodology followed here mathematically searches for the approximate solution for the motion equations of the GMA with the PPF damper, which has been accomplished by using one of the most famous perturbation methods. The multiple scale perturbation technique (MSPT) of the second-order approximation is our strategy to obtain the analytical results. The stability of the system has also been investigated and observed by implementing frequency response equations to close the concurrent primary and internal resonance cases. By utilizing Matlab and Maple programs, all numerical discussions have been accomplished and explained. The resulting influence on the amplitude due to changes in the parameters' values has been studied by the frequency response curves. Finally, a comparison between both the analytical and numerical solutions using time history and response curves is made. In addition to the comparison between our PPF damper's effect on the GMA, previous works are presented. To get our target in this article, we have mentioned some important applications utilized in the GMA system just to imagine the importance of controlling the GMA vibration.

Keywords: vibration control; GMA; frequency response equation; stability; PPF control; multiple scale perturbations
Mathematics Subject Classification: 34A34, 37N35, 70J99, 70K20, 74H10

1. Introduction

It has become clear how important it is to dampen the vibrations occurring in different engineering mechanical structures. Given the importance of this topic, many researchers have been working on how to control these vibrations and improve their ability to reduce the amplitude of these vibrations in the worst cases of resonance. Giant magnetostrictive materials (GMM) are considered very famous engineering structures that are a sort of utilitarian materials created since the 1970s, denoted by their high energy density and vast magnetostrain. A presentation of magnetostriction and the historical backdrop of magnetostrictive materials is portrayed. Besides, we audit the new advancements of both uncommon and common earth magnetostrictive materials. Contrasted and other cunning materials, GMM has a high Curie temperature, high attractive mechanical coupling coefficient, quick reaction, and vast magnetostrictive strain [1,2]. In addition, another phase of actuators employing the magnetostrictive impact for driving GMM as a driving force to change over electromagnetic energy into mechanical energy is called the giant magnetostrictive actuator (GMA). GMAs are generally used to perform power harvesting, control mechanical vibrations, drive electrohydraulic servovals, and rate microelectromechanical systems [3–8].

Notwithstanding, since the GMM pole has the issue of hysteresis nonlinear peculiarity, there is a nonlinear connection in the middle of the applied attractive field, and the resulting strain of the GMA, which truly obliterates the nonlinear soundness of the GMA [9–11]. Generally speaking, to direct the plan of the GMA structure, execution assessment, control, and applying the GMA in various implementations are important to complete the exploration of the GMA nonlinear stability. In conclusion, scientists have proposed assorted plans, including the robust control as Nealis & Smith presented [12], optimal control that was introduced by Oates & Smith [13], self-adaptivetive control algorithm explained by Wang et al. [14], and applied H-infinity robust control described by Liu et al. [15] to decrease and damp the impact of nonlinear elements on yield stability. Moreover, Hong et al. [16] applied two controllers to dominate the nonlinear mechanical behaviors in a more detailed chaotic motion, where principal resonance response and amplitude of the GMA system has been expressed mathematically as a one degree of freedom. They introduced a thorough study of the system, and in this work, a numerical comparison has been held between the effect of all controllers. Under the parametric excitations, Wei [17] investigated the nonlinear characteristics of the MEMS in addition to bifurcation and chaos.

El-Sayed and Bauomy [18,19] concentrated on the exhibitions of the PPF approach for decreasing the motions of an upward transport. They detailed that the PPF presented can diminish the vibration of the approaching framework. Additionally, they presented the effect of the Nonlinear Integral Positive Position Feedback (NIPPF) to decrease the high vibration amplitude of the system. Omidi et al. [20] presented the impact of the multi-positive input approach on piezoelectric-actuated flexible constructions. According to the outcomes, the presentation of a multi positive feedback damper is more proficient in decreasing vibration than the MPPF damper. A consensus modified positive position feedback (CMPPF) is discovered by decentralizing and disseminating the modified positive position feedback (MPPF) to a network of control agents, which has been presented by Qi et al. [21] to reduce the large flexible structure oscillation in the spacecraft. Hamed et al. [22] investigated the nonlinear vibrations, stability, and resonance of a cantilever using a new nonlinear MPPF approach.

The PPF control technique implemented by Jun [23] is an effective strategy for suppressing the high amplitude response of a flexible beam subjected to primary external excitation. Additionally, the PPF controller is applied to the structure of a flexible manipulator with a collocated piezoelectric sensor/actuator pair. The active vibration control of clamp beams is investigated by Shin et al. [24].

They used multiple PPF controllers with a sensor/moment pair actuator to overcome the problems of instability. It is illustrated both numerically and experimentally that the vibration levels are brought down at the tuned modes of the PPF controllers. El-Ganaini et al. [25] elaborated a nonlinear dynamic model subjected to external primary resonance excitation. They used the PPF controller to suppress the vibration amplitude of the system. The PPF controller is applied to control the vibrations at all resonant modes using piezoelectric sensor voltage feedback.

Amer et al. [26] applied the PPF to dampen the vibration of the MEMS. They studied the worst resonance case treating the vibrating system and observed the effect of parameters on the main system and the PPF. Yaghoub and Jamalabadi [27] studied the suppression of mechanical oscillations of the galloping system using the PPF controller. The results show that the PPF controller is a powerful method to decrease the galloping amplitude of the D-shaped prism. Bauomy and El-Sayed [28] considered the nonlinear dynamic vibrations of a composite plate with square and cubic nonlinear terms exposed to external and parametric excitations. This system is controlled using three PPF controllers, thus they have a new six-degree-of-freedom model. The techniques of PPF and PDF controllers were applied by Syed [29] on a single-link flexible manipulator featuring a piezoelectric actuator. Based on the studied system, the comparison between the two controllers has concluded that the PDF controller is overall more effective in repressing vibrations than the PPF controller. Responses of the closed-loop system for NIPPF, IRC, and PPF controllers are explained, and the stability analysis was performed by Omidi and Mahmoodi [30]. Applying NIPPF reveals that the vibration amplitude is sufficiently suppressed at the exact resonant frequency and the corresponding peaks in the frequency domain are also greatly reduced compared to the other two controllers. Therefore, the NIPPF controller produces the greatest efficiency in the frequency and time domains. El-Sayed and Bauomy [31] investigated the effect NIPPF faces when ANIPPF is applied to the shearer's semi-direct drive cutting transmission system. They found out from this investigation that the ANIPPF controller equips the superior system control. All these results are proved analytically and numerically. A NSC simulation was used for reducing the vibrations of the nonlinear cantilever beam by Bauomy and El-Sayed [32]. They used a perturbation analysis to find out the mathematical solution; then, they compared it to the numerical solution. Amer et al. [33] used the positive position feedback to control the vibration of the nonlinear spring pendulum. They applied the multiple scale method in the mathematical solution to get the frequency response equation and studied the effect of parameters. Bauomy and El-Sayed [34] controlled the vibration of the macro-fiber composite by connecting a nonlinear proportional-derivative. They achieved high effectiveness in applying this damper. According to Fang, Ma, and Zhu [35], the coupling constitutive relation is derived from the piezoelectric semiconductor one-dimensional phenomenological theory. It has also beed discovered that the performance of electronic devices can be controlled by altering the electric potential and concentration from positive to negative in the nanofiber. On the basis of Reddy higher order shear deformation theory and von Kármán geometric nonlinearity assumption, the relationship between nonlinear free vibration behavior and nonlinear forced vibration behavior of viscoelastic plates was explored by Fang, Zhu, and Liu [36]. The main originality of the text was that the nonlinear frequency ratio calculated from the system's nonlinear free vibration agrees well with the resonant frequency ratio derived from the system's nonlinear forced vibration. Moreover, the nonlinear frequency ratio is slightly influenced by the viscous damping coefficient.

In the light of the above-mentioned aspects, the current paper focuses on examining the problem of the vibrations motion of GMA system via PPF control action to avoid high amplitudes. The amplitude is decreased in the current work from the actual value without control by 84.5%. The multiple scale perturbation technique (MSPT) methodology is sufficiently significant to set out toward

getting second-order close to the system's arrangements. All possible resonances are removed at this estimation request demand. The demeanor of the framework is represented numerically either before or after applying the damper. The stability investigation is numerically accomplished for all the frequency response curves to get stable and unstable zones for each curve in the case of the simultaneous primary and internal resonance cases $\left(\omega = \omega_0, \omega_0 = \omega_1\right)$, which is the worst resonance case. The effects of the few boundaries and the edge work led to the mentioned resonance case by the propagation results organized by the Matlab 7.0 programming.

Finally, the numerical results have explained the first-class concurrence with the mathematical ones. As indicated by these outcomes, we have introduced a correlation between this paper and the accessible contemporary papers illustrating the upsides of utilizing the PPF regulator with this framework.

2. GMA system model

The essential construction of the GMA framework, displayed in Figure 1, is for the most part made of an attractive circuit structure, a preload gadget, and a result gadget.

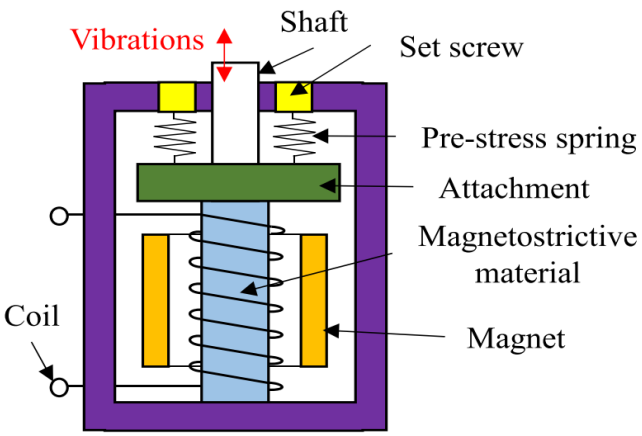

Figure 1. Structural schematic of GMA.

The nonlinear second-order ordinary differential equation that acquaints for the equation of motion for the GMA is deduced in Ref. [16] as:

$$\ddot{x} + 2\hat{\mu}\dot{x} + \omega_0^2 x + \hat{\beta}_1 x^2 + \hat{\beta}_2 x^3 = \hat{f}\, cos(\omega t), \tag{2.1}$$

a mathematical expression formula of the PPF damper, shown in Figure 2 and designed especially for tightening control over the GMA, is presented as follows:

$$\ddot{u} + 2\hat{\mu}_1\dot{u} + \omega_1^2 u = \hat{G}_2 x. \tag{2.2}$$

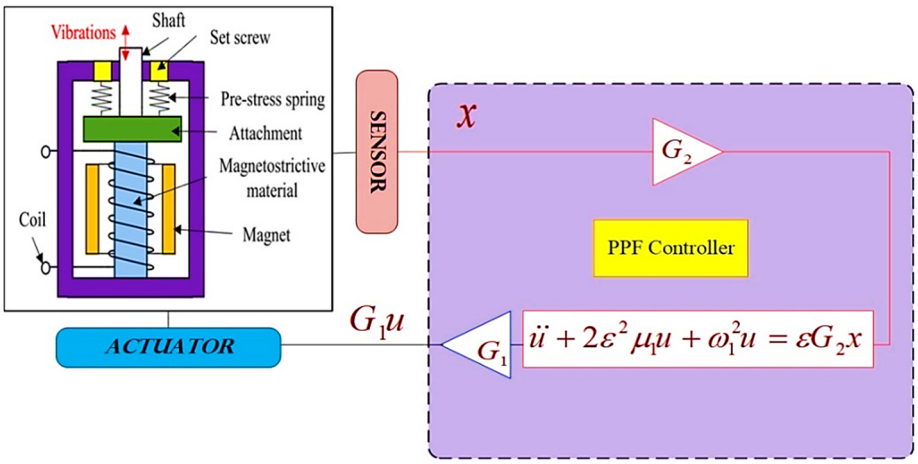

Figure 2. Improved the model of the GMA framework with PPF controller.

3. Perturbation analysis

To expedite the perturbation methodology, the previous equations will be written in the posterior formulas:

$$\ddot{x}+2\varepsilon^2\mu\dot{x}+\omega_0^2 x+\varepsilon\beta_1 x^2+\varepsilon^2\beta_2 x^3=\varepsilon^2 f\cos(\omega t)+\varepsilon^2 G_1 u, \tag{3.1a}$$

$$\ddot{u}+2\varepsilon^2\mu_1\dot{u}+\omega_1^2 u=\varepsilon^2 G_2 x, \tag{3.1b}$$

where μ and μ_1 are the coefficient of damping for the GMA and the PPF damper, respectively, ω_0 and ω_1 are defined as the natural frequencies for both GMA and PPF, respectively, f and ω are the external excitation force and the frequency of the framework, respectively, β_1 and β_2 are nonlinear parameters, G_1 and G_2 are gains, and ε is a small perturbation parameter.

To find out the 2nd order approximate solutions for Eqs (3.1a) and (3.1b) using the MSPT [37,38] after adding PPF damper to the GMA

$$x\left(T_0,T_1,T_2,\varepsilon\right)=x_0\left(T_0,T_1,T_2\right)+\varepsilon x_1\left(T_0,T_1,T_2\right)+\varepsilon^2 x_2\left(T_0,T_1,T_2\right), \tag{3.2a}$$

$$u\left(T_0,T_1,T_2,\varepsilon\right)=u_0\left(T_0,T_1,T_2\right)+\varepsilon u_1\left(T_0,T_1,T_2\right)+\varepsilon^2 u_2\left(T_0,T_1,T_2\right), \tag{3.2b}$$

where ε is a sufficiently significant perturbation parameter ($0<\varepsilon<1$), $T_m=\varepsilon^m t$ and the derivatives, $D_m=\dfrac{\partial^m}{\partial T_m}, m=0,1,2$, so, the derivatives for time formulas will be realized as

$$\frac{d}{dt}=D_0+\varepsilon D_1+\varepsilon^2 D_2, \tag{3.3a}$$

$$\frac{d^2}{dt^2}=D_0^2+\varepsilon(2D_0D_1)+\varepsilon^2(D_1^2+2D_0D_2), \tag{3.3b}$$

Equating the coefficients of equal power ε after substituting from Eqs (3.2a) to (3.3b) into Eqs (3.1a) and (3.1b), will procure to:

Order ε^0:

$$(D_0^2 + \omega_0^2)x_0 = 0, \tag{3.4a}$$

$$(D_0^2 + \omega_1^2)u_0 = 0. \tag{3.4b}$$

Order ε^1:

$$(D_0^2 + \omega_0^2)x_1 = -2D_0D_1x_0 - \beta_1 x_0^2, \tag{3.5a}$$

$$(D_0^2 + \omega_0^2)u_1 = -2D_0D_1u_0. \tag{3.5b}$$

Order ε^2:

$$\left(D_0^2 + \omega_0^2\right)x_2 = -2D_0D_1x_1 - D_0^2x_0 - 2D_0D_2x_0 - 2\mu D_0x_0 - 2\beta_1(x_0x_1)$$
$$-\beta_2 x_0^3 + f\cos(\omega t) + G_1u_0, \tag{3.6a}$$

$$(D_0^2 + \omega_1^2)u_2 = -2D_0D_1u_1 - D_1^2u_0 - 2D_0D_2u_0 - 2\mu_1 D_0u_0 + G_2x_0. \tag{3.6b}$$

The general solution of the Eqs (3.4a) and (3.4b)

$$x_0 = Ae^{i\omega_0T_0} + \bar{A}e^{-i\omega_0T_0}, \tag{3.7a}$$

$$u_0 = Be^{i\omega_1T_0} + \bar{B}e^{-i\omega_1T_0}, \tag{3.7b}$$

where, A and B represent complex functions in T_1. Substituting (3.7a) and (3.7b) into (3.5a) and (3.5b), we obtain

$$(D_0^2 + \omega_0^2)x_1 = \left[-2i\omega_0D_1A\right]e^{i\omega_0T_0} - \beta_1A^2e^{2i\omega_0T_0} - \beta_1A\bar{A} + cc., \tag{3.8a}$$

$$\left(D_0^2 + \omega_1^2\right)u_2 = -2i\omega_1D_1Be^{i\omega_1T_0} + cc., \tag{3.8b}$$

$cc.$ locates for the complex conjugate of the preceding terms.

Then, we can say that the Eqs (3.9a) and (3.9b) can be considered as the solution of Eqs (3.8a) and (3.8b)

$$x_1 = \frac{\beta_1A^2}{3\omega_0^2}e^{2i\omega_0T_0} - \frac{\beta_1A\bar{A}}{\omega_0^2} + cc., \tag{3.9a}$$

$$u_2 = 0. \tag{3.9b}$$

Substituting Eqs (3.9a) and (3.9b) into Eqs (3.6a) and (3.6b), we obtain:

$$\left(D_0^2 + \omega_0^2\right)x_2 = R_1e^{i\omega_0T_0} + R_2e^{2i\omega_0T_0} + R_3e^{3i\omega_0T_0} + R_4e^{i\omega_1T_0} + R_5e^{i\omega T_0} + cc., \tag{3.10a}$$

$$(D_0^2 + \omega_1^2)u_2 = L_1 e^{i\omega_1 T_0} + L_2 e^{i\omega_0 T_0} + cc.. \tag{3.10b}$$

From Eqs (3.7a), (3.7b), (3.9a), (3.9b), (3.10a), and (3.10b), we can put the secular terms as follow:

Order ε^0:

$$D_1 A = 0, \tag{3.11a}$$

$$D_1 B = 0. \tag{3.11b}$$

Order ε^1:

$$D_1^2 A = 0, \tag{3.11c}$$

$$D_1^2 B = 0. \tag{3.11d}$$

Order ε^2:

$$\left[-D_1^2 A - 2\mu(i\omega_0)A - 2(i\omega_0)D_2 A + \frac{10\beta_1^2 A^2 \bar{A}}{3\omega_0^2} - 3\beta_1 A^2 \bar{A}\right] e^{i\omega_0 T_0} + \frac{f}{2} e^{i\omega_1 T_0} + G_1 B e^{i\omega T_0} = 0, \tag{3.11e}$$

$$[-D_1^2 B - 2i\omega_1 D_2 B - 2i\mu_1 \omega_1 B] e^{i\omega_1 T_0} + G_2 A e^{i\omega_0 T_0} = 0. \tag{3.11f}$$

From these resonances' cases, we have estimated the thought about the simultaneous resonances $\omega \cong \omega_0; \omega_1 \cong \omega_0$ as the worst one of other resonance cases. Additionally, in the next section, we will be seeking the stability of the estimated resonance methodically and numerically, respectively.

3.1 The periodic solution

The stability analysis of the altered plate is matured in a simultaneous resonance case, $\omega \cong \omega_0; \omega_1 \cong \omega_0$. These cases after resonance conditions are in the following form:

$$\begin{cases} \omega = \omega_0 + \varepsilon^2 \sigma_1, \\ \omega_1 = \omega_0 + \varepsilon^2 \sigma_2, \end{cases} \tag{3.12}$$

where σ_1 and σ_2 are named as detuning parameters.

Inserting Eq (3.12) into secular and slight-divisor terms, starting the first oncoming in Eq (3.11) toward solvability conditions, we get:

$$2i\omega_0 D_1 A = 0, \tag{3.13a}$$

$$2i\omega_0 D_1 B = 0, \tag{3.13b}$$

$$2i\omega_0 D_2 A = -D_1^2 A - 2i\mu\omega_0 A + \frac{10\beta_1^2 A^2 \bar{A}}{3\omega_0^2} - 3\beta_2 A^2 \bar{A} + \frac{f}{2} e^{i\sigma_1 T_2} + G_1 B e^{i\sigma_2 T_2}, \tag{3.13c}$$

$$2i\omega_1 D_2 B = -D_1^2 B - 2i\mu_1\omega_1 B + G_2 A e^{i\sigma_2 T_2}. \tag{3.13d}$$

To get the solution of Eq (3.13), we state as:

$$\begin{cases} A = \dfrac{1}{2} a e^{i\varphi}, \\ B = \dfrac{1}{2} b e^{i\theta}, \end{cases} \tag{3.14}$$

where, a, b, φ, and θ are steady-state amplitude and phases of motion, respectively. Embedding Eq (3.14) into Eq (3.13), following which we equate real and imaginary elements then:

$$\dot{a} = \varepsilon^2 \left[-\mu a + \frac{f}{2\omega_0} \sin\gamma_1 + \frac{G_1}{2\omega_0} b \sin\gamma_2 \right], \tag{3.15a}$$

$$a\dot{\varphi} = \varepsilon^2 \left[-\frac{5\beta_1^2 a^3}{12\omega_0^3} + \frac{3\beta_2 a^3}{8\omega_0} - \frac{f}{2\omega_0} \cos\gamma_1 - \frac{G_1}{2\omega_0} b \cos\gamma_2 \right], \tag{3.15b}$$

$$\dot{b} = -\mu_1 b - \frac{G_2}{2\omega_1} a \sin\gamma_2, \tag{3.15c}$$

$$b\dot{\theta} = -\frac{G_2}{2\omega_1} a \cos\gamma_2, \tag{3.15d}$$

where $\gamma_1 = \sigma_1 T_2 - \phi, \gamma_2 = i\sigma_2 T_2 + \theta - \phi$.

3.2 Frequency response equations (FREs)

Steady-state solution of the GMA system using PPF controllers linked to the fixed point of (3.15a)–(3.15d) be gained at $\dot{a} = 0, \dot{b} = 0$, and $\dot{\gamma}_n = 0$, then the FREs of the practical case $(a \neq 0, b \neq 0)$ are given by:

$$0 = \varepsilon^2 \left[-\mu a + \frac{f}{2\omega_0} \sin\gamma_1 + \frac{G_1}{2\omega_0} b \sin\gamma_2 \right], \tag{3.16a}$$

$$a\sigma_1 = -\left(\frac{10\beta_1^2 - 9\omega_0^2\beta_2}{24\omega_0^3} \right) a^3 + \left[-\frac{f}{2\omega_0} \cos\gamma_1 - \frac{G_1}{2\omega_0} b \cos\gamma_2 \right], \tag{3.16b}$$

$$0 = -\mu_1 b - \frac{G_2}{2\omega_1} a \sin\gamma_2, \tag{3.16c}$$

$$b(\sigma_1 - \sigma_2) = -\frac{G_2}{2\omega_1} a \cos\gamma_2. \tag{3.16d}$$

Quadrangle and adding together for (3.16a)–(3.16d), then:

$$\left(\mu a+\frac{G_1\omega_1\mu_1 b^2}{G_2\omega_0 a}\right)^2+\left(a\sigma_1+\frac{10\beta_1^2-9\omega_0^2\beta_2}{24\omega_0^3}a^3+\frac{G_1 b^2\omega_1(\sigma_1-\sigma_2)}{G_2 a\omega_0}\right)^2=\frac{f^2}{4\omega_0^2}, \tag{3.17a}$$

$$\mu_1^2 b^2+b^2(\sigma_1-\sigma_2)^2=\tfrac{G_2^2}{4\omega_2^2}a^2. \tag{3.17b}$$

4. Stability at the fixed point

For incorporating the stability analysis of the steady-state solution, we begin:

$$\begin{cases} a=a_0+a_1, \\ b=b_0+b_1, \\ \gamma_m=\gamma_{m0}+\gamma_{m1}\,(m=1,2), \end{cases} \tag{4.1}$$

where a_0, b_0, and γ_{m0} are the solutions of (3.15a)–(3.15d) and a_1, b_1, and γ_{m1} are perturbations which are assumed small compared with a_0, b_0, and γ_{m0}. Substituting from Eq (4.1) into Eqs (3.15a)–(3.15d) and keeping only the linear terms of a_1, b_1, and γ_{m1}, we get the following equations:

$$\dot{a}_1=[-\mu]a_1+\left[\frac{f}{2\omega_0}\cos\gamma_{10}\right]\gamma_{11}+\left[\frac{G_1}{2\omega_0}\sin\gamma_{20}\right]b_1+\left[\frac{G_1}{2\omega_0}b_0\cos\gamma_{20}\right]\gamma_{21}, \tag{4.2a}$$

$$\dot{\gamma}_1=\left[\frac{\sigma_1}{a_0}+\frac{\left(10\beta_1^2-9\omega_0^2\beta_2\right)}{8\omega_0^3}\right]a_1+\left[\frac{-f}{2\omega_0 a_0}\sin\gamma_{10}\right]\gamma_{11}+\left[\frac{G_1}{2\omega_0 a_0}\cos\gamma_{20}\right]b_1+\left[\frac{-G_1}{2\omega_0 a_0}b_0\sin\gamma_{20}\right]\gamma_{21}, \tag{4.2b}$$

$$\dot{b}_1=\left[-\frac{G_2}{2\omega_1}\sin\gamma_{20}\right]a_1+[0]\gamma_{11}+[-\mu_1]b_1+\left[-\frac{G_2}{2\omega_1}a_0\cos\gamma_{20}\right]\gamma_{21}, \tag{4.2c}$$

$$\dot{\gamma}_2=\left[\frac{\sigma_1}{a_0}+\frac{10\beta_1^2-9\omega_0^2\beta_2}{8\omega_0^3}a_0-\frac{G_2}{2\omega_0 b_0}\cos\gamma_{20}\right]a_1+\left[\frac{-f}{2\omega_0 a_0}\sin\gamma_{10}\right]\gamma_{11}+\left[\frac{\sigma_2-\sigma_1}{b_0}+\frac{G_1}{2\omega_0 a_0}\cos\gamma_{20}\right]b_1$$
$$+\left[\frac{G_2}{2\omega_1 b_0}a_0\sin\gamma_{20}-\frac{G_2}{2\omega_0 a_0}b_0\sin\gamma_{20}\right]\gamma_{21}. \tag{4.2d}$$

We can express these equations as the following matrix:

$$\begin{bmatrix}\dot{a}_1\\ \dot{\gamma}_1\\ \dot{b}_1\\ \dot{\gamma}_2\end{bmatrix}=\begin{bmatrix}R_{11}&R_{12}&R_{13}&R_{14}\\ R_{21}&R_{22}&R_{23}&R_{24}\\ R_{31}&R_{32}&R_{33}&R_{34}\\ R_{41}&R_{42}&R_{43}&R_{44}\end{bmatrix}\begin{bmatrix}a_1\\ \gamma_1\\ b_1\\ \gamma_1\end{bmatrix} \tag{4.3}$$

where the system's Jacobian matrix coefficients are given in (4.2). The eigenvalue equations below can be written as:

$$\begin{vmatrix} R_{11}-\lambda & R_{12} & R_{13} & R_{14} \\ R_{21} & R_{22}-\lambda & R_{23} & R_{24} \\ R_{31} & R_{32} & R_{33}-\lambda & R_{34} \\ R_{41} & R_{42} & R_{43} & R_{44}-\lambda \end{vmatrix} = 0 . \tag{4.4}$$

Expanding the determinant at (4.4), yields

$$\lambda^4 + \Gamma_1\lambda^3 + \Gamma_2\lambda^2 + \Gamma_3\lambda + \Gamma_4 = 0 \tag{4.5}$$

where λ is the eigenvalue of the matrix, $\Gamma_1, \Gamma_2, \Gamma_3$ and Γ_4 are coefficients of (4.5). If the real part of the eigenvalue is negative according to the Routh-Hurwitz criterion, the periodic solution is stable; otherwise, it is unstable.

5. Results and discussion

5.1 Numerical Solutions with time history

Figures 3 and 4 displayed the numerical recreation outright for a time-history of the considered GMA framework without and with PPF controllers by preparing the Runge-Kutta fourth arranged calculation inside the worst resonance case at the following selected values: $(\omega_1 = \omega_0; \omega_0 = 2; \mu = 0.07; \beta_1 = 0.05; \beta_2 = 1; f = 0.8; G_1 = 3; \ \mu_1 = 0.005; G_2 = 2; \sigma_2 = 0)$.

From Figure 3, the steady-state amplitudes for the GMA framework (x) without any controllers have higher values within the considered synchronous reverberation case. After including the PPF controller, the steady state amplitude decreased to exceptionally little esteem in Figure 4; this clarifies that the effectiveness of the control E_a (E_a=amplitude of the system before control/ amplitude of the system after control) is about 6.241. Poincare map for the GMA system before and after the PPF controller can be drawn as shown in Figure 5.

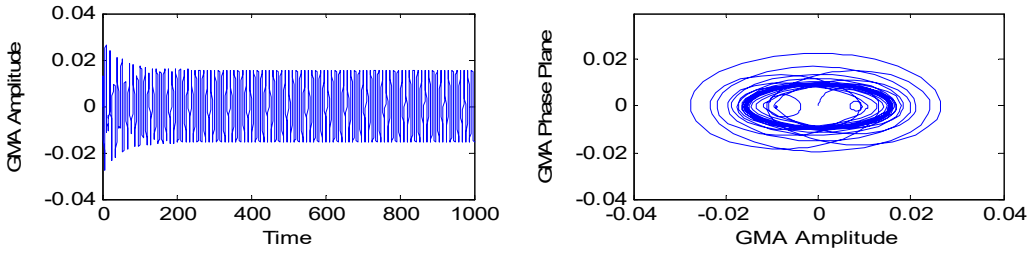

Figure 3. Time history diagram and phase trajectory of the uncontrolled GMA system.

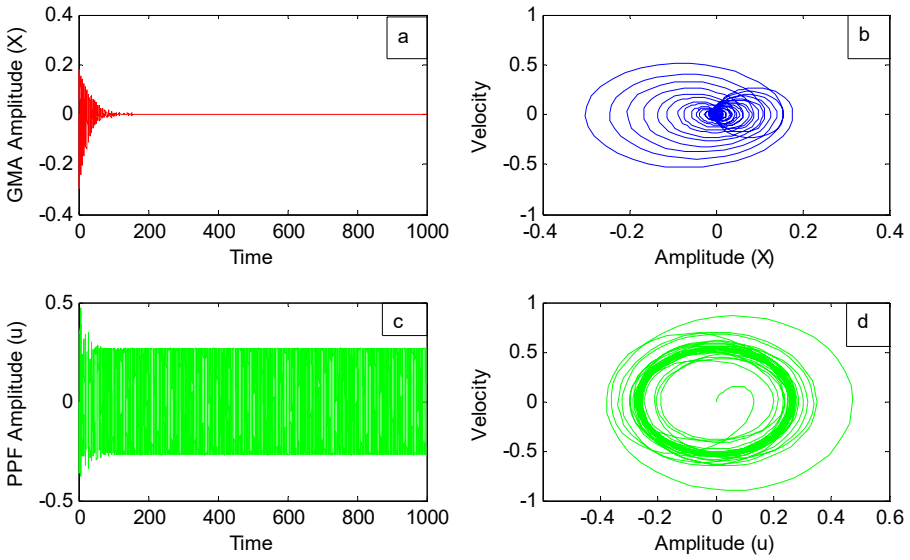

Figure 4. GMA system x with PPF controllers u at ($\omega \cong \omega_0; \omega_1 \cong \omega_0$). (a) Waveform for x. (b) Phase plane for x. (c) Waveform for u. (d) Phase plane for u.

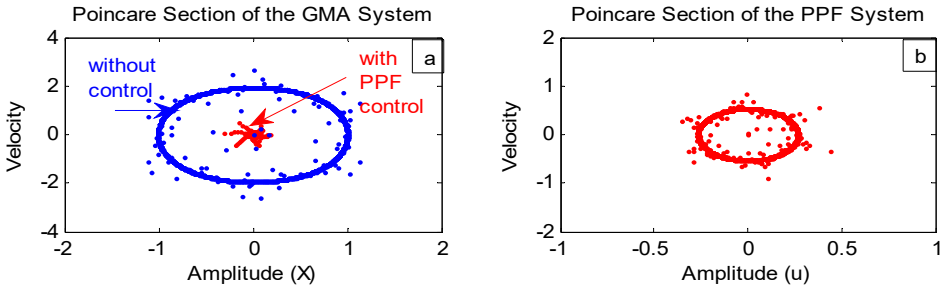

Figure 5. Comparison between the main GMA system and the system with PPF control using Poincare map. (a) Comparison between the system before and after control. (b) GMA system with PPF control.

5.2 Comparison between numerical simulation and frequency response curves

To verify the validity of the obtained results in Figure 4, a comparison is made between the modulation amplitude of the system x, the controller u from the frequency response curve (presented by line) from one side, and the amplitude of the system with the controller from the Runge–Kutta 4th order numerical method (addressed by the closed circles) at the case $\dot{a}=0, \dot{b}=0$, and $\dot{\gamma}_n = 0$ with $a \neq 0, b \neq 0$ from the other side. Then, we get a good effect in Figures 6 and 7.

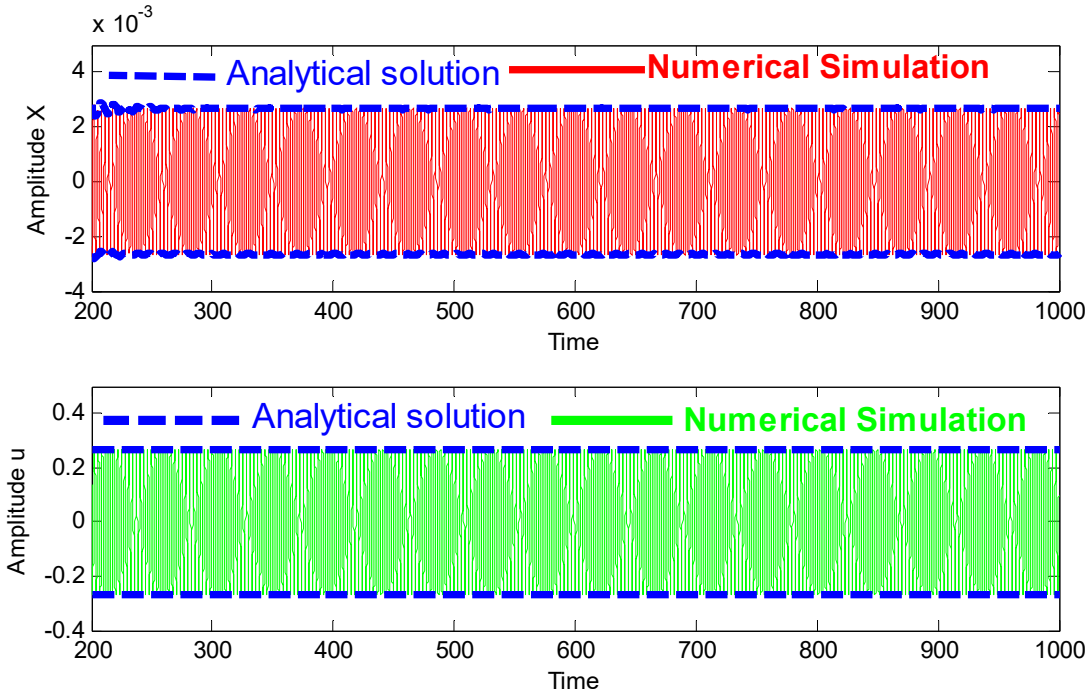

Figure 6. Comparison between perturbation analysis and numerical simulation of the mGMA system within PPF-controllers.

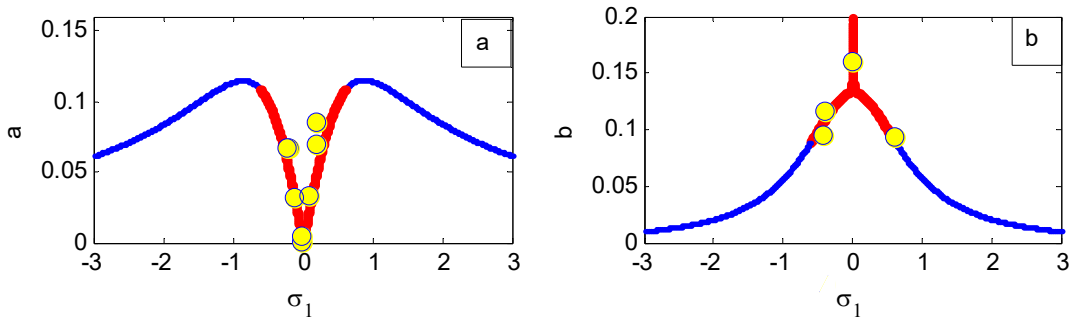

Figure 7. Comparison between amplitudes from the frequency response curves (line) and Runge-Kutta method (closed circle) (a) the first part of the GMA system (*a*) (b) is the associated control (*b*).

5.3 Outcomes and discussion

Graphics (2D and 3D) included here are based on measurements resulting from the harmonic balance method. 2D episodes consist of heavy-colored branches (i.e., stable solutions) or light-colored branches (i.e., unstable solutions) due to Floquet's theoretical analysis. 3D episodes contain spaces that provide a typical 2D episode feature. To the learner's knowledge, the upper area is depicted in a dark red color, while the bottom is shown in a dark blue color.

In this segment, we have examined the nonlinear Eqs (3.16) and (3.17), which discuss the frequency response equations at $\dot{a}=0,\dot{b}=0$, and $\dot{\gamma}_n=0$, with $a\neq 0,b\neq 0$. In all figures, the green light line is compared to the unsteady locale; something else characterizes the steady locale at clear values of coefficients. Figure 8 demonstrates FRCs for the GMA system with amplitude a and the corresponding PPF control amplitude b against detuning parameter σ_1.

Figure 8 reveals the amplitude with little esteem occurrence, which in turn endorses the proficiency of the PPF control to decrease the measured reverberation vibration. Figure 9 shows that the small values of the natural frequency ω_0 of the GMA system are small unstable regions, but for the bigger value the unstable region appears, and the bandwidth of the curve decreased. Moving from Figure 9a to Figure 9b and from Figure 9c to Figure 9d, it is apparent that the GMA amplitude a as a work of both a and b detuning parameter σ_1 within the shape of a 3D surface in arrange shows a wide viewpoint of the bends plotted in Figure 9a and 9c. Figure 10 announces the perception of the GMA framework, wherein changing the values of the damping coefficient μ, at $\mu=0.07$ and $\mu=0.02$ the amplitudes coincide with each other, but after raising the esteem of μ with little sum, the amplitude diminishes. This happened with the framework a and the controller b and shows up in Figure 10(a,c) with 2D plots. Figure 10(b–d) pronounced the same result with 3D charts, as displayed in ruddy color with tall adequacy and in a blue color with little amplitude. Figure 11(a,c) and Figure 12(a,c) reveal the impact of the non-dimensional second-order stiffness term coefficient β_1 of the GMA framework, and the third-arrange solidness term coefficient β_2 of the GMA spring on the frequency response curve, declaring no alteration of the amplitude of the framework and the controller while changing the values of the coefficients. Figure 11(b,d) and Figure 12(b,d) pronounce that the amplitudes of the GMA system have the same esteem at distinctive values of stiffness coefficients, as affirmed by a 3D plot. In Figure 13(a,c), the GMA vibration amplitude a and the controller b respond to the detuning parameter σ_1 at multiple excitation forces f. The curves grow with a high value of forces, making a more unstable region with high amplitude; however, for the diminished values of the external forces, the amplitude of the GMA system decreases gradually, and the effect appears to be due to the spring's hardening phenomenon. Moving from Figure 13(a,c) to Figure 13(b,d), it is noticeable that the GMA amplitude a acts as a function of σ_1 and is portrayed in the shape of a 3D surface, displaying the wide aspect of the curves plotted in Figure 13(b,d).

Figure 14(a,b) illustrated the effect of the damping coefficient μ_1 for GMA against the amplitude of the system a. For the least esteem of μ_1, the amplitude of the GMA system is not high; however, at the moment of expanding μ_1 values, the circulation of the figure turns up and appears in 3D portion of Figure 14(b). On the other side, Figure 14(c,d) clarify that for small μ_1, the amplitude of the GMA controllers b is exceptionally low with the little stable region and delivers a high amplitude with the expanding value of μ_1, saving a large stable region in both 2D and 3D figures. For the gains' impact of the GMA system and the controller G_1 and G_2, respectively, we find that in

Figure 15(a,b) and Figure 16(a,b) the smaller gains value and the high amplitudes are given, whether for the system or the controller with discrete points of the stable region in 2D. Figure 15(b,d) and Figure 16(b,d) are 3D figures of G_1 and G_2 of the GMA model, respectively. We think that these plots give fascinating behavior for the parameters that shows how the amplitude decreases and increases in an applicable way. As shown in Figure 17(a,c), when σ_2 changes from 0 to 3, the resonance curve of the GMA is exposed to a right bending case (hardening phenomenon). A left bending case (softening phenomenon) σ_2 is in the range from -3 to 0 is seen in Figure 17(b,d), where the 3D figure approved and clarified the action of the detuning parameters.

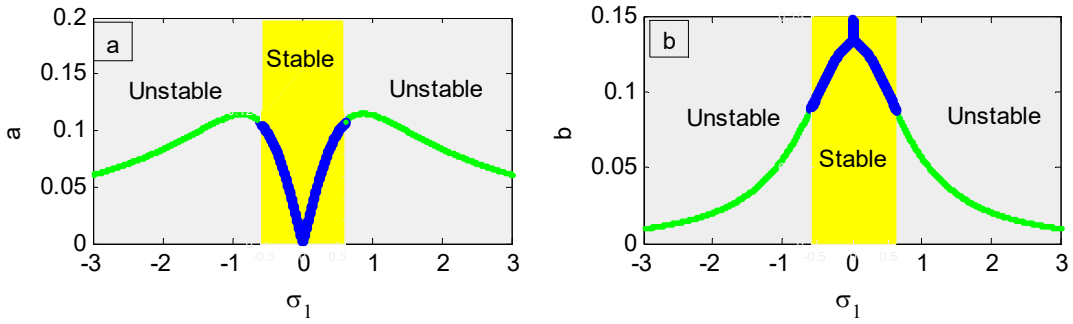

Figure 8. The frequency response curve of the system (σ_1 . amplitude) (a) the first part of the system (*a*) (b) is the associated control (*b*).

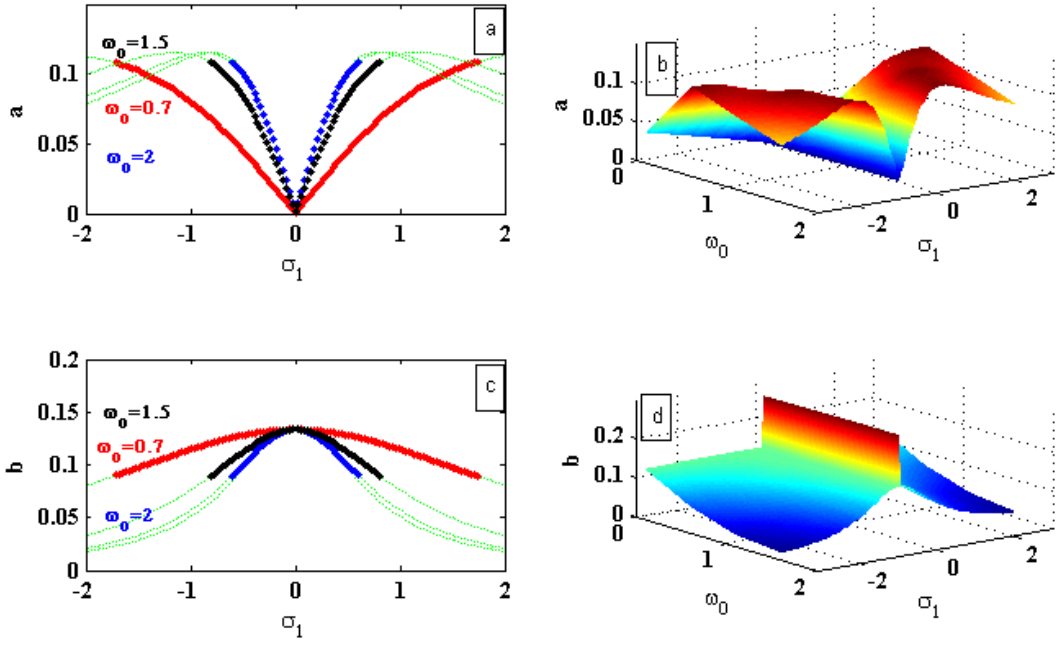

Figure 9. The frequency response curve of the system (σ_1 . amplitude) at different values of ω_0 (a, b) the 2D and 3D viewing with the first part of the system (*a*) (c, d) the 2D and 3D viewing with the associated control (*b*).

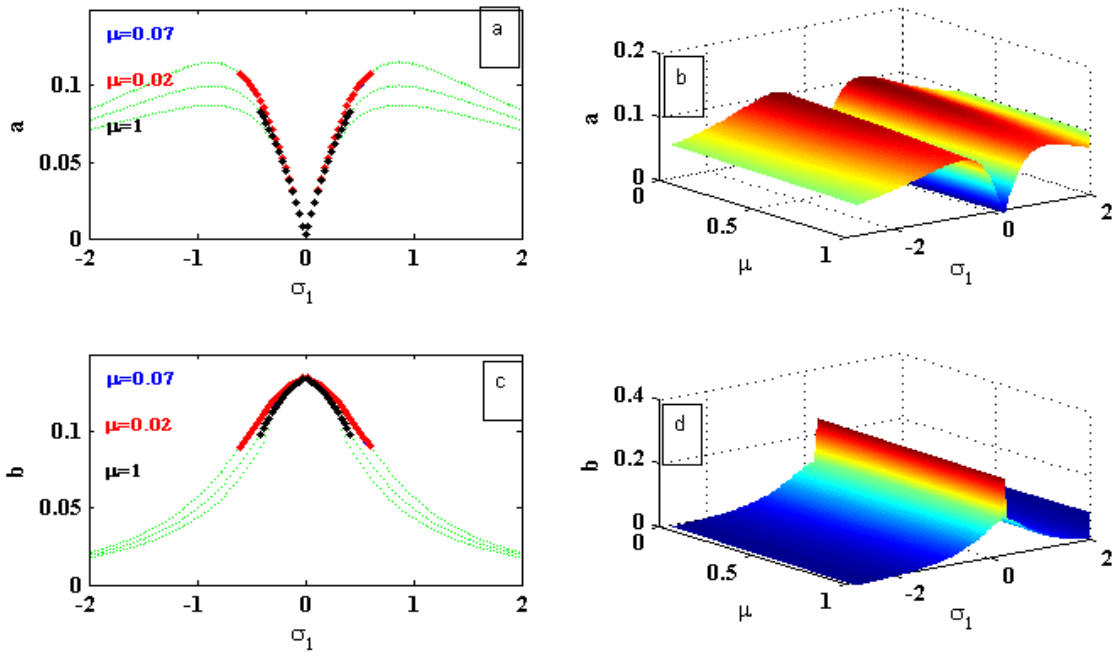

Figure 10. The frequency response curve of the system (σ_1 . amplitude) at different values of μ (a, b) the 2D and 3D viewing with the first part of the system (*a*), (c, d) the 2D and 3D viewing with the associated control (*b*).

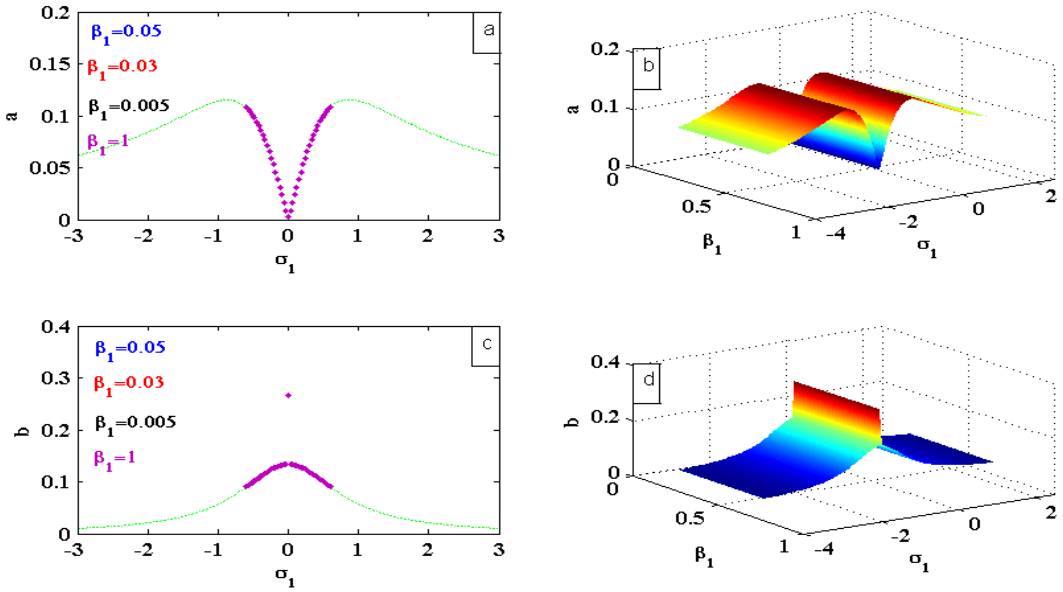

Figure 11. The frequency response curve of the system (σ_1 . amplitude) at different values of β_1 (a, b) the 2D and 3D viewing with the first part of the system (*a*), (c, d) the 2D and 3D viewing with the associated control (*b*).

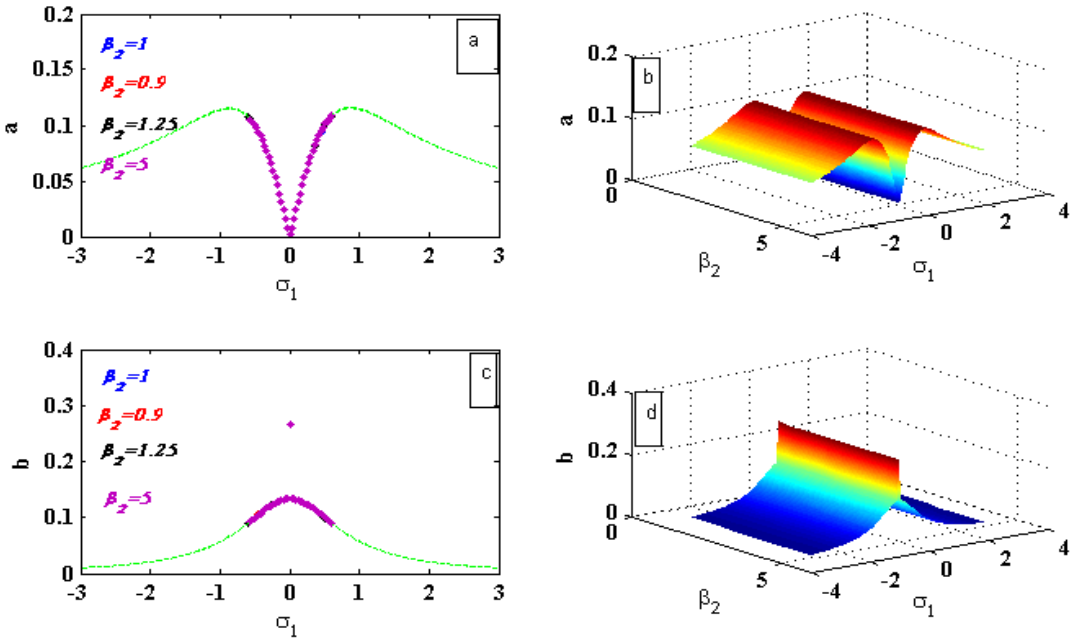

Figure 12. The frequency response curve of the system (σ_1 . amplitude) at different values of β_2 (a, b) the 2D and 3D viewing with the first part of the system (*a*), (c, d) the 2D and 3D viewing with the associated control (*b*).

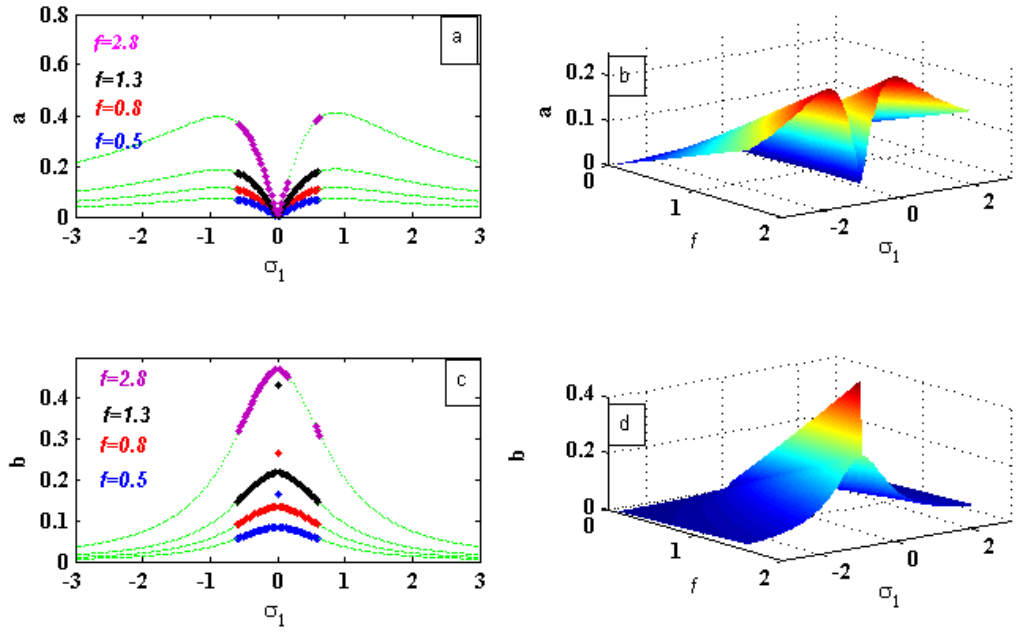

Figure 13. The frequency response curve of the system (σ_1 . amplitude) at different values of f (a, b) the 2D and 3D viewing with the first part of the system (*a*), (c, d) the 2D and 3D viewing with the associated control (*b*).

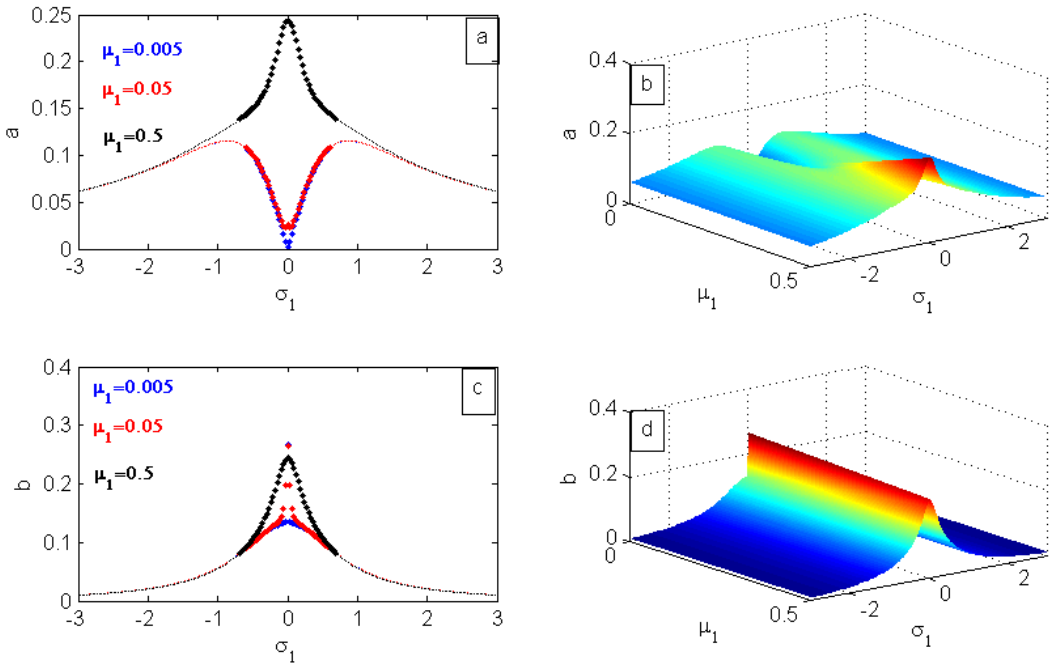

Figure 14. The frequency response curve of the system (σ_1 . amplitude) at different values of μ_1 (a, b) the 2D and 3D viewing with the first part of the system (*a*), (c, d) the 2D and 3D viewing with the associated control (*b*).

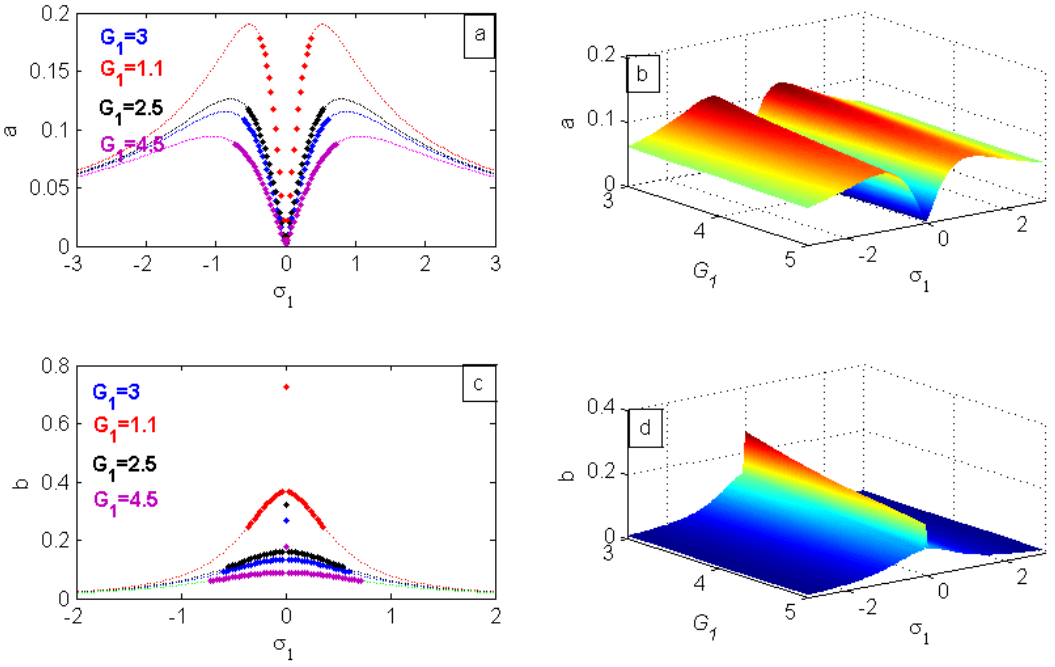

Figure 15. The frequency response curve of the system (σ_1 . amplitude) at different values of G_1 (a, b) the 2D and 3D viewing with the first part of the system (*a*), (c, d) the 2D and 3D viewing with the associated control (*b*).

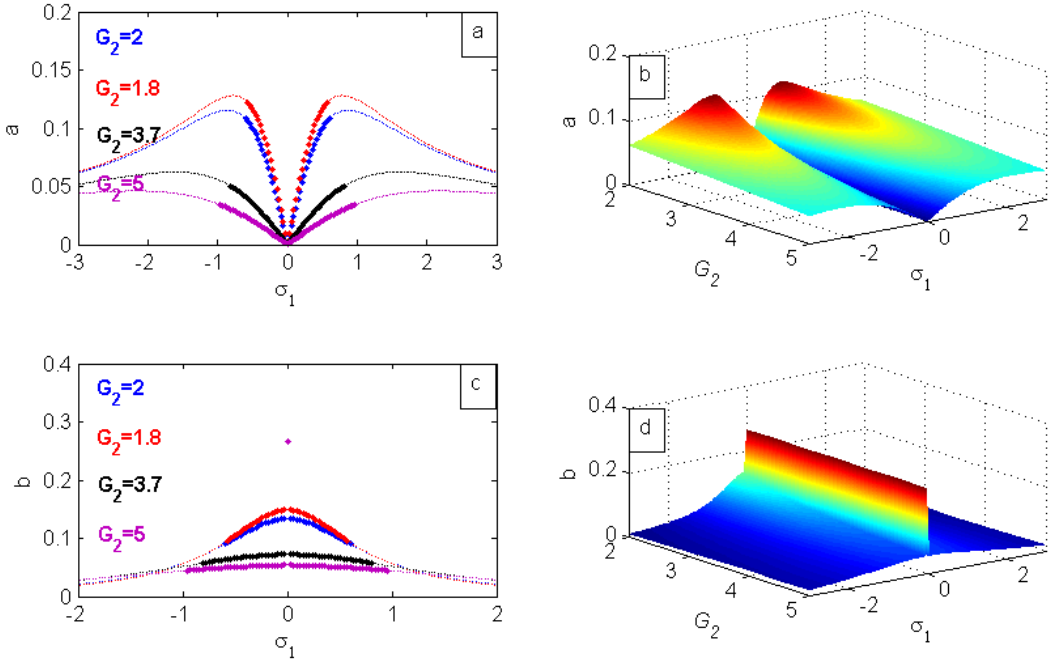

Figure 16. The frequency response curve of the system (σ_1 . amplitude) at different values of G_2 (a, b) the 2D and 3D viewing with the first part of the system (*a*), (c, d) the 2D and 3D viewing with the associated control (*b*).

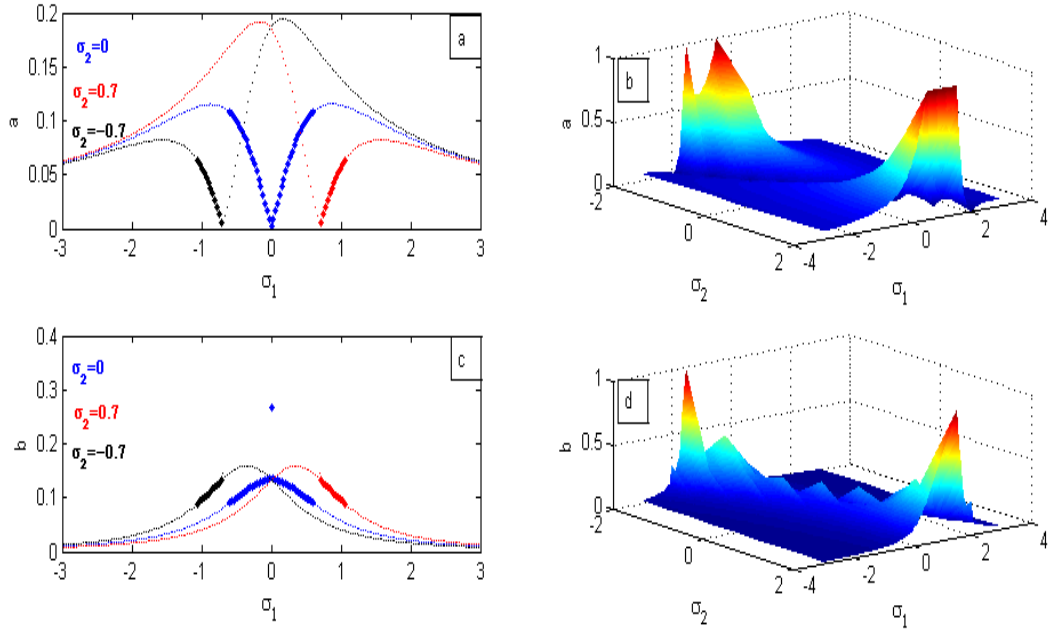

Figure 17. The frequency response curve of the system (σ_1 . amplitude) at different values of σ_2 (a, b) the 2D and 3D viewing with the first part of the system (*a*), (c, d) the 2D and 3D viewing with the associated control (*b*).

6. Comparison with available published work

The creator in Ref. [16] has presented how the GMA system behaved with time-delayed displacement and a velocity feedback controller with particularly principal resonance response, where the stability is considered, and the multi-scale method is utilized.

In this review, we have modified the system by adding a PPF controller system that made sense by two degrees of freedom with a primary resonance case, thus prevailing with regards in lessening the vibrations in the same system appropriately. The discussed frequency response curves in the deliberate case with new related controls for the system has illustrated the regions of the stability and vibration bandwidth at different values of the system and control factors. This examination is clearer by drawing the connection between the time and the amplitude of the system, endorsing that the new control has improved the amplitude and made the system more stable than the previous work (Figure 18).

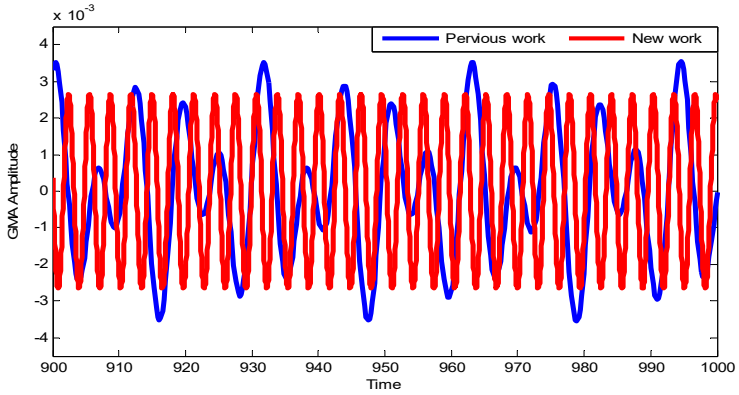

Figure 18. comparison between the previous work and this study.

7. Conclusions

This work has managed to utilize a controlled GMA model with addressed conditions using the multi-scale strategy. The effect of the PPF controller has been tried for stability examination, which in turn has been satisfied to regard the stable and unstable regions of such a model's behavior in the wake of applying the control unit. Then, 2D and 3D graphical plots have also been incorporated to consider the conditions coming about because of the multi-scale strategy. Additionally, a mathematical reproduction has been performed involving the fourth request Runge-Kutta strategy to affirm the largely controlled conduct of the model concentration. The entire work can be summed up in the following focuses:

1) In the case of the small value of the natural frequency ω_0 of the GMA system, there is a small unstable region, but for a bigger value the unstable region appears and the bandwidth of the curve decreases.
2) After raising the esteem of μ with little sum, the amplitude diminishes. This happens with the framework a and the controller b.
3) The impact of the non-dimensional second-order stiffness term coefficient of the GMA framework β_1 and third-arrange solidness term coefficient β_2 of the GMA spring on the frequency response curve reveal that there are no alterations to the amplitude of the framework or the controller when changing the values of the coefficients.

4) For the high value of forces f, more unstable regions with high amplitude appear, but for the little values of the external forces f, the amplitude of the GMA system decreases gradually, and the effect appears due to the spring's hardening phenomenon.
5) The results show that for the least esteem of μ_1, the amplitude of GMA system is not high but, when expanding μ_1 values, the circulation of the figure turns up.
6) For the smaller gains values of G_1 and G_2, the high amplitudes are given, whether for the system or the controller, with discrete points of the stable region.
7) When σ_2 changes from 0 to 3, the resonance curve of the GMA is exposed to a right bending case (hardening phenomenon). A left bending case (softening phenomenon) for σ_2 is in the range from -3 to 0.

To sum up, in this article we have laid out the PPF control of the nonlinear GMA framework. The stability of the essential resonance and the amplitude of the framework could be productively constrained by tuning the PPF boundaries. A few examinations have been made to affirm the legitimacy of the outcomes. The eventual outcomes have been contrasted with the past work and showed how the effectiveness of the framework got to the next level. The 3D plot has also been laid out to improve the work and show its exactness.

Acknowledgements

This study is supported via funding from Prince sattam bin Abdulaziz University project number (PSAU/2023/R/1444).

Conflict of interest

The authors declare that there are no conflicts of interest.

References

1. J. Liu, C. Jiang, H. Xu, Giant magnetostrictive materials, *Sci. China Technol. Sci.*, **55** (2012), 1319–1326. https://doi.org/10.1007/s11431-012-4810-0
2. F. Claeyssen, N. Lhermet, R. Le Letty, P. Bouchilloux, Actuators, transducers, and motors based on giant magnetostrictive materials, *J. Alloys Compd.*, **258** (1997), 61–73. https://doi.org/10.1016/S0925-8388(97)00070-4
3. L. Zhu, X. Cao, Y. Lu, Design method and characteristics study on actuator of giant magnetostrictive Harmonic motor, *J. Mech. Eng.*, **54** (2018), 204–211. https://doi.org/10.3901/JME.2018.22.204
4. Z. W. Fang, Y. W. Zhang, X. Li, H. Ding, L. Q. Chen, Integration of a nonlinear energy sink and a giant magnetostrictive energy harvester, *J. Sound Vib.*, **391** (2017), 35–49. https://doi.org/10.1016/j.jsv.2016.12.019
5. Y. Zhu, Y. Li, Development of a deflector-jet electrohydraulic servovalve using a giant magnetostrictive material, *Smart Mater. Struct.*, **23** (2014), 115001. https://doi.org/10.1088/0964-1726/23/11/115001

6. G. Xue, P. Zhang, Z. He, D. Li, Z. Yang, Z. Zhao, Displacement model and driving voltage optimization for a giant magnetostrictive actuator used on a high-pressure common-rail injector, *Mater. Design*, **95** (2016), 501–509. https://doi.org/10.1016/j.matdes.2016.01.139
7. J. Zhou, Z. He, C. Rong, G. Xue, A giant magnetostrictive rotary actuator: design, analysis and experimentation, *Sensors Actuat. A: Phys.*, **287** (2019), 150–157. https://doi.org/10.1016/j.sna.2018.12.031
8. G. Xue, P. Zhang, Z. He, B. Li, C. Rong, Design and model for the giant magnetostrictive actuator used on an electronic controlled injector, *Smart Mater. Struct.*, **26** (2017), 05LT02. https://doi.org/10.1088/1361-665X/aa69a1
9. X. Gao, Y. Liu, Research on control strategy in giant magnetostrictive actuator based on Lyapunov stability, *IEEE Access*, **7** (2019), 77254–77260. https://doi.org/10.1109/ACCESS.2019.2920853
10. Y. Liu, X. Gao, Y. Li, Giant magnetostrictive actuator nonlinear dynamic Jiles–Atherton model, *Sensors Actuat. A: Phys.*, **250** (2016), 7–14. https://doi.org/10.1016/j.sna.2016.09.009
11. G. Xue, P. Zhang, X. Li, Z. He, H. Wang, Y. Li, et al., A review of giant magnetostrictive injector (GMI), *Sensors Actuat. A: Phys.*, **273** (2018), 159–181. https://doi.org/10.1016/j.sna.2018.02.001
12. J. M. Nealis, R. C. Smith, Robust control of a magnetostrictive actuator, *Smart Structures and Materials 2003: Modeling, Signal Processing, and Control*, **5049** (2003), 221–232. https://doi.org/10.1117/12.482738
13. W. S. Oates, R. C. Smith, Nonlinear optimal control of plate structures using magnetostrictive actuators, *Smart Structures and Materials 2005: Modeling, Signal Processing, and Control*, **5757** (2005), 281–291. https://doi.org/10.1117/12.602270
14. L. Wang, J. B. Tan, Y. T. Liu, Research on giant magnetostrictive micro-displacement actuator with self-adaptive control algorithm, *J. Phys.: Conf. Ser.*, **13** (2005), 446–449. https://doi.org/10.1088/1742-6596/13/1/103
15. P. Liu, J. Q. Mao, Q. S. Liu, K. M. Zhou, Modeling and H-infinity robust control for giant magnetostrictive actuators with rate-dependent hysteresis, *Control Theory Appl.*, **30** (2013), 148–155. https://doi.org/10.7641/CTA.2013.20794
16. H. Gao, Z. Deng, Y. Zhao, H. Yan, X. Zhang, L. Meng, et al., Time-delayed feedback control of nonlinear dynamics in a giant magnetostrictive actuator, *Nonlinear Dyn.*, **108** (2022), 1371–1394. https://doi.org /10.1007/s11071-022-07265-1
17. W. Zhang, G. Meng, K. Wei, Dynamic characteristics of electrostatically actuated MEMS under parametric excitations, *Chinese J. Theor. Appl. Mech.*, **41** (2009), 282–288. https://doi.org /10.6052/0459-1879-2009-2-2007-598
18. A. T. El-Sayed, H. S. Bauomy, Nonlinear analysis of vertical conveyor with positive position feedback (PPF) controllers, *Nonlinear Dyn.*, **83** (2016), 919–939. https://doi.org/10.1007/s11071-015-2377-6
19. A. T. El-Sayed, H. S. Bauomy, Outcome of special vibration controller techniques linked to a cracked beam, *Appl. Math. Model.*, **63** (2018), 266–287. https://doi.org/10.1016/j.apm.2018.06.045
20. E. Omidi, S. N. Mahmoodi, W. S. Shepard Jr, Multi positive feedback control method for active vibration suppression in flexible structures, *Mechatronics*, **33** (2016), 23–33. https://doi.org/10.1016/j.mechatronics.2015.12.003

21. N. Qi, Q. Yuan, Y. Liu, M. Huo, S. Cao, Consensus vibration control for large flexible structures of spacecraft with modified positive position feedback control, *IEEE Trans. Control Syst. Technol.*, **27** (2018), 1712–1719. https://doi.org/10.1109/TCST.2018.2830301
22. Y. S. Hamed, A. El Shehry, M. Sayed, Nonlinear modified positive position feedback control of cantilever beam system carrying an intermediate lumped mass, *Alex. Eng. J.*, **59** (2020), 3847–3862. https://doi.org/10.1016/j.aej.2020.06.039
23. L. Jun, Positive position feedback control for high-amplitude vibration of a flexible beam to a principal resonance excitation, *Shock Vib.*, **17** (2010), 187–203. https://doi.org/10.3233/SAV-2010-0506
24. C. Shin, C. Hong, W. B. Jeong, Active vibration control of clamped beams using positive position feedback controllers with moment pair, *J. Mech. Sci. Technol.*, **26** (2012), 731–740. https://doi.org/10.1007/s12206-011-1233-y
25. W. A. El-Ganaini, N. A. Saeed, M. Eissa, Positive position feedback (PPF) controller for suppression of nonlinear system vibration, *Nonlinear Dyn.*, **72** (2013), 517–537. https://doi.org/10.1007/s11071-012-0731-5
26. Y. A. Amer, A. T. EL-Sayed, A. M. Salem, Vibration control in MEMS resonator using positive position feedback (PPF) controller, *J. Adv. Math.*, **12** (2016), 6821–6834. https://doi.org/10.24297/jam.v12i11.1114
27. M. Y. A. Jamalabadi, Positive position feedback control of a galloping structure, *Acoustics*, **1** (2019), 47–58. https://doi.org/10.3390/acoustics1010005
28. H. S. Bauomy, A. T. EL-Sayed, A new six-degrees of freedom model designed for a composite plate through PPF controllers, *Appl. Math. Model.*, **88** (2020), 604–630. https://doi.org/10.1016/j.apm.2020.06.067
29. H. H. Syed, Comparative study between positive position feedback and negative derivative feedback for vibration control of a flexible arm featuring piezoelectric actuator, *Int. J. Adv. Robotic Syst.*, **14** (2017), 1–9. https://doi.org/10.1177/1729881417718801
30. E. Omidi, S. N. Mahmoodi, Sensitivity analysis of the nonlinear integral positive position feedback and integral resonant controllers on vibration suppression of nonlinear oscillatory systems, *Commun. Nonlinear Sci. Numer. Simul.*, **22** (2015), 149–166. https://doi.org/10.1016/j.cnsns.2014.10.011
31. A. T. EL-Sayed, H. S. Bauomy, NIPPF versus ANIPPF controller outcomes on semi-direct drive cutting transmission system in a shearer, *Chaos, Solitons Fract.*, **156** (2022), 111778. https://doi.org/10.1016/j.chaos.2021.111778
32. H. Bauomy, A. Taha, Nonlinear saturation controller simulation for reducing the high vibrations of a dynamical system, *Math. Biosci. Eng.*, **19** (2022), 3487–3508. https://doi.org/10.3934/mbe.2022161
33. Y. A. Amer, A. T. EL-Sayed, F. T. El-Bahrawy, Positive position feedback controllers for reduction the vibration of a nonlinear spring pendulum, *J. Adv. Math.*, **12** (2016), 6758–6772. https://doi.org/10.24297/jam.v12i11.7
34. H. S. Bauomy, A. T. El-Sayed, Act of nonlinear proportional derivative controller for MFC laminated shell, *Phys. Scripta*, **95** (2020), 095210. https://doi.org/10.1088/1402-4896/abaa7c
35. X. Q. Fang, H. W. Ma, C. S. Zhu, Non-local multi-fields coupling response of a piezoelectric semiconductor nanofiber under shear force, *Mech. Adv. Mater. Struct.*, 2023, 1–8. https://doi.org/10.1080/15376494.2022.2158503

36. C. S. Zhu, X. Q. Fang, J. X. Liu, Relationship between nonlinear free vibration behavior and nonlinear forced vibration behavior of viscoelastic plates, *Commun. Nonlinear Sci. Numer. Simul.*, **117** (2023), 106926. https://doi.org/10.1016/j.cnsns.2022.106926
37. A. H. Nayfeh, *Perturbation methods*, New York: Wiley, 2000. https://doi.org/10.1002/9783527617609
38. A. H. Nayfeh, D. T. Mook, *Nonlinear oscillations*, New York: Wiley, 1995. https://doi.org/10.1002/9783527617586

Appendix

$$R_1 = \left[-D_1^2 A - 2\mu(i\omega_0)A - 2(i\omega_0)D_2 A + \frac{10\beta_1^2 A^2 \bar{A}}{3\omega_0^2} - 3\beta_1 A^2 \bar{A} \right]$$

$$R_2 = \left[-\frac{4\beta_1(i\omega_0)}{3\omega_0} D_1 A^2 \right]$$

$$R_3 = \left[\frac{-2\beta_1^2 A^3}{3\omega_0^2} - \beta_2 A^3 \right]$$

$$R_4 = \frac{f}{2}, R_5 = G_1 B$$

$$L_1 = \left[-D_1^2 B - 2i\omega_1 D_2 B - 2i\mu_1\omega_1 B \right]$$

$$L_2 = G_2 A$$

AIMS Press

© 2023 the Author(s), licensee AIMS Press. This is an open access article distributed under the terms of the Creative Commons Attribution License (http://creativecommons.org/licenses/by/4.0)